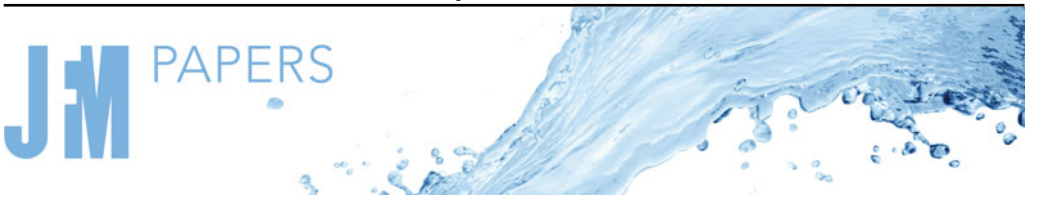
J. Fluid Mech. (2026), *vol.* 1026, A9, doi:10.1017/jfm.2025.10999



Theoretical analysis of Stokes flow through a sharp-cornered cross-slot

Xintong Ji[1], **Helen J. Wilson**[1] **and Elena Luca**[2]

[1]Department of Mathematics, University College London, Gower Street, London WC1E 6BT, UK

[2]Climate and Atmosphere Research Center, The Cyprus Institute, Nicosia 2121, Cyprus

Corresponding author: Xintong Ji, xintong.ji.22@ucl.ac.uk

(Received 31 March 2025; revised 16 September 2025; accepted 25 November 2025)

We consider the flow of a viscous fluid through a two-dimensional symmetric cross-slot geometry with sharp corners. The problem is analysed using the unified transform method in the complex plane, providing a quasi-analytical solution that can be used to compute all the physical quantities of interest. This study is a novel application of this method to a complicated geometry featuring multiple sharp corner singularities and multiple inlets and outlets. Our approach offers the advantage of resolving unbounded domains, as well as providing quantities of interest, such as the velocity and stress profiles, and the Couette pressure correction, from the solution of low-order linear systems. Our results agree well with the existing literature, which has largely used truncated bounded geometries with rounded or curved corners.

Key words: low-Reynolds-number flows, microfluidics, computational methods

1. Introduction

Low Reynolds number flow is of increasing importance in a wide range of applications, as the science of miniaturisation is progressing and small-scale 'lab-on-a-chip' devices become more widespread for applications, from DNA analysis to drug discovery (e.g. Manz, Lee & Wheeler 2021; Wang & Kelley 2025; Xu *et al.* 2025). As a result, there is a growing focus on the two-dimensional Stokes flow problem, which involves solving the biharmonic equation (Langlois 1964), in complicated geometries.

A variety of mathematical methods have been developed to solve the biharmonic equation in planar domains. A historical overview of topics related to the classical two-dimensional biharmonic problem and some analytical approaches to its solution

© The Author(s), 2025. Published by Cambridge University Press. This is an Open Access article, distributed under the terms of the Creative Commons Attribution licence (https://creativecommons.org/licenses/by/4.0/), which permits unrestricted re-use, distribution and reproduction, provided the original article is properly cited.

https://doi.org/10.1017/jfm.2025.10999 Published online by Cambridge University Press

was given by Meleshko (2003). Two-dimensional Stokes flow problems are accessible analytically in special cases, when the geometry and boundary conditions are simple enough. Dean & Montagnon (1949) and Moffatt (1964) used separation of variables in plane polar coordinates to analyse Stokes flow near a corner region. For problems in channel geometries, series expansions using Papkovich–Fadle eigenfunctions in rectangular regions have been used extensively (Joseph 1977; Joseph & Sturges 1978; Kim & Chung 1984; Phillips 1989; Jeong 2001*a*; Setchi *et al.* 2013). In addition, for flows in channels in which the ratio of the channel width to length is very small, the solution can be approximated by lubrication theory (Ockendon & Ockendon 1995; Howison 2005), as well as extended lubrication theory (Tavakol *et al.* 2017). Moreover, even though the biharmonic equation is not conformally invariant (Langlois 1964), conformal mapping techniques have been used to solve two-dimensional Stokes flow problems successfully in some special geometries (Crowdy & Samson 2010; Crowdy 2013*a*,*b*).

Another group of classical methods for solving Stokes flow problems consists of transform methods. Davis (1993) presented the solution to various problems involving point singularities in a channel using Fourier transforms. The Wiener–Hopf technique, which relies on Fourier transforms and the factorisation of functions into upper- and lower-analytic ones, can be used to analyse problems involving mixed boundary conditions. Jeong (2001*b*) analysed the flow around a semi-infinite wall in a symmetric channel divider using the Wiener–Hopf technique; in this case, the analysis led to a scalar Wiener–Hopf problem that was then solved analytically. Abrahams, Davis & Llewellyn Smith (2008) considered Stokes flow in an asymmetric channel divider; in this case, the boundary value problem was reduced to a matrix Wiener–Hopf problem that was solved using Padé approximants. Kim & Chung (1984) analysed the flow in a channel with a finite plate parallel to the walls using a three-part Wiener–Hopf formulation.

To the best of our knowledge, all the present work using the above analytical or quasi-analytical methods focuses on relatively simple geometries. In more complicated geometries, there are a rich variety of numerical methods for the solution of boundary value problems for the biharmonic equation: boundary integral techniques (Pozrikidis 1987, 1992; Roure, Zinchenko & Davis 2024), finite difference methods (Strikwerda 1984), finite element methods (Logg, Mardal & Wells 2012) and the lattice Boltzmann method (Krüger *et al.* 2017). For flows in domains with sharp corners, these numerical methods require careful analysis near corners, e.g. mesh refinement, with expensive computational cost. It is also common to round the corners with a small radius of curvature (Hellou & Bach 2011; Cruz *et al.* 2014) or to simply ignore the singularity behaviour near the corners. More recently, a new method, known as the lightning-AAA rational Stokes (LARS) algorithm, has been developed to solve two-dimensional Stokes flow problems (Xue *et al.* 2024, 2025) in bounded or truncated bounded geometries. The LARS algorithm was established on the basis of the lightning algorithm that uses rational functions to approximate functions when solving harmonic (Gopal & Trefethen 2019) and biharmonic (Brubeck & Trefethen 2022) equations in polygons with only straight lines as boundaries, and the AAA (adaptive Antoulas–Anderson) algorithm (Nakatsukasa, Sète & Trefethen 2018; Costa & Trefethen 2023) that computes rational approximations on curved boundaries.

In this study, we consider Stokes flow through the sharp-cornered cross-slot (or cross-channel), as shown in figure 1. This is the first work to use a quasi-analytical method to solve Stokes flow through a complicated geometry with multiple sharp corner singularities and multiple inlets and outlets. The cross-slot has four 'arms', with the inflow coming from two opposite (horizontal) 'arms', and the outflow going away from the other two opposite (vertical) 'arms'. A slow flow through the cross-slot produces a pattern with reflectional

https://doi.org/10.1017/jfm.2025.10999 Published online by Cambridge University Press

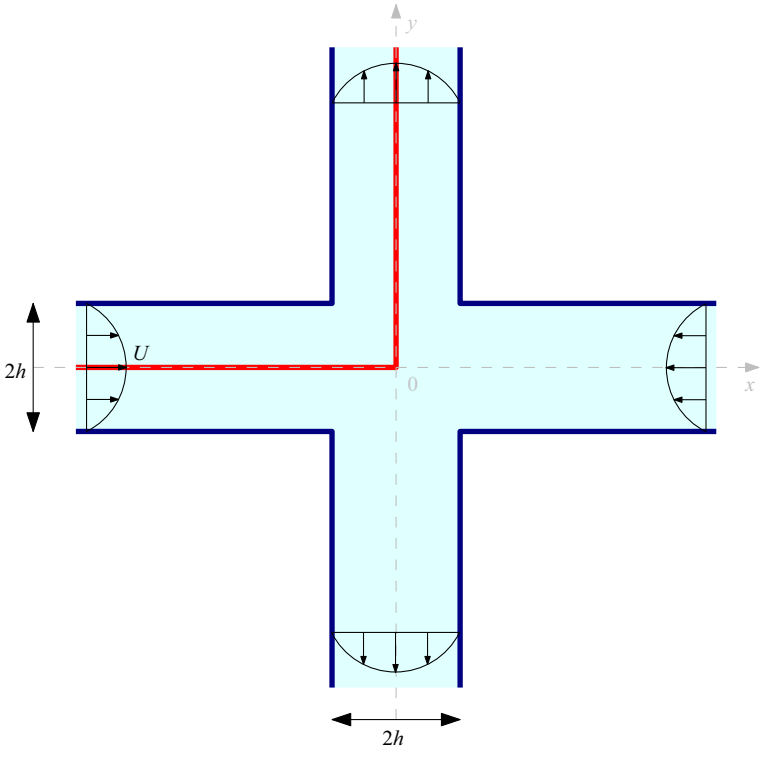


Figure 1. Schematic of the pressure-driven flow through a sharp-cornered cross-slot geometry. A custom coordinate system based on the central line (red) is introduced with coordinate ℓ monotonically increasing from inlet ($\ell = -\infty$) to origin ($\ell = 0$) to outlet ($\ell = \infty$).

symmetry, and produces a good approximation to a pure planar extension near the stagnation point at the centre; therefore, this flow geometry is widely used in rheometry to measure the extensional viscosity of fluids (Odell & Carrington 2006; Alves 2008; Haward *et al.* 2012). The cross-slot flow involves a complicated mixture of shear and extension even in the two-dimensional case. One reason why the cross-slot device has come to prominence in recent years is the discovery of a symmetry-breaking event in viscoelastic cross-slot flow as the flow rate is increased, which is understood to be a purely elastic instability. In particle-tracking experiments (Arratia *et al.* 2006), this non-Newtonian instability behaviour of viscoelastic cross-slot flow was initially observed at very low Reynolds numbers. Numerical simulations using finite-volume methods based on different models (Poole, Alves & Oliveira 2007; Rocha *et al.* 2009; Cruz *et al.* 2014; Davoodi, Domingues & Poole 2019) were then conducted to support the experimental results, and further conclude that this purely elastic flow instability is generated by non-uniform polymer chain extension along the curvilinear streamlines. In chemical engineering, this cross-slot flow instability is effective in mixing processes (Galindo-Rosales, Alves & Oliveira 2013). The flow geometry can also be widely found in microfluidic chips and other devices in material, biological and electronic engineering (Squires & Quake 2005; Dylla-Spears *et al.* 2010; Yeo *et al.* 2011).

The aim of this study is to provide a theoretical foundation and analytical insights for the two-dimensional sharp-cornered cross-slot Stokes flow problem. We solve the problem using the unified transform method (UTM), also known as the Fokas method, which is a method for solving linear and integrable nonlinear partial differential equations (Fokas

https://doi.org/10.1017/jfm.2025.10999 Published online by Cambridge University Press

1997, 2008). This method provides a generalisation of the classical Fourier transform, since it involves simultaneous spectral analysis with respect to two independent variables x and y (i.e. in the complex plane). The UTM has been successfully used to solve various biharmonic boundary value problems arising in the study of Stokes flow and plane elasticity, in convex polygonal (Crowdy & Fokas 2004; Crowdy & Davis 2013; Crowdy & Luca 2014; Dimakos & Fokas 2015; Crowdy & Brzezicki 2017; Luca & Llewellyn Smith 2018) and circular (Luca & Crowdy 2018) domains. There is a series of advantages over the purely numerical approaches mentioned above, due to the quasi-analytical nature of our method, including the ability to resolve unbounded domains without truncation, the good computational accuracy without any meshing or refined local analysis near the problematic corner singularities, and the fast computational speed on a standard laptop by solving low-order linear systems. All physical quantities of interest are computed via the UTM, from the solution of low-order linear systems, which is the first attempt at investigating the use of this method in solving a complicated geometry. In particular, we compare the pressure drop from the inlets to the outlets of the cross-slot geometry with fully developed flow in the straight channel to address the Couette correction, as well as computing velocity and stress profiles. We compare the solution under different conditions with all, some or no imposed symmetry conditions to investigate computational accuracy. This will also establish a theoretical foundation for Stokes flow problems in further complicated geometries with sharp corners.

2. Complex variable formulation of Stokes flow

Stokes flow with dominant viscous effects and negligible inertial effects ($Re \to 0$) is governed by the Stokes equations as

$$\left.\begin{array}{l} -\boldsymbol{\nabla} p + \eta_s \, \nabla^2 \boldsymbol{u} = 0, \\ \boldsymbol{\nabla} \cdot \boldsymbol{u} = 0, \end{array}\right\} \tag{2.1}$$

where $p = p(\boldsymbol{x})$ denotes the dynamic pressure, η_s is the solvent viscosity, and $\boldsymbol{u} = \boldsymbol{u}(\boldsymbol{x})$ is the velocity field. For two-dimensional flow, we have the pressure as $p = p(x, y)$ and the velocity field as $\boldsymbol{u} = \boldsymbol{u}(x, y) = (u(x, y), v(x, y))$. The vorticity field, denoted as $\boldsymbol{\omega}(x, y)$, is defined as the curl of velocity $\boldsymbol{u}(x, y)$:

$$\boldsymbol{\omega}(x, y) := \boldsymbol{\nabla} \times \boldsymbol{u}(x, y), \tag{2.2}$$

with $\boldsymbol{\omega}(x, y) = (0, 0, \omega(x, y))$, where the direction of the vorticity ω is out of the plane of the velocity field. The stream function, denoted as ψ, is a scalar function, which is a constant along each streamline (fixed for steady flow), with definition

$$\boldsymbol{u}(x, y) := \boldsymbol{\nabla} \times (0, 0, \psi(x, y)) = \left(\frac{\partial \psi}{\partial y}, -\frac{\partial \psi}{\partial x} \right), \tag{2.3}$$

in Cartesian coordinates. It can be deduced from (2.1) that ψ is a biharmonic function:

$$\nabla^4 \psi(x, y) = 0. \tag{2.4}$$

The two-dimensional system (2.1) expressed in terms of coordinates (x, y) can be changed into a system in terms of $(z, \overline{z})$, introducing the complex variable $z = x + \mathrm{i}y$ and its complex conjugate $\overline{z} = x - \mathrm{i}y$. The biharmonic (2.4) becomes

$$\frac{\partial^4 \psi}{\partial z^2 \, \partial \overline{z}^2} = 0, \tag{2.5}$$

https://doi.org/10.1017/jfm.2025.10999 Published online by Cambridge University Press

which has general solution (Langlois 1964) of the form

$$\psi\,(z,\overline{z}) = \mathrm{Im}\big[\overline{z}\,f(z) + g(z)\big], \tag{2.6}$$

where both $f(z)$ and $g(z)$ are analytic (but can have isolated singularities) in the interior of the fluid region, and

$$4f'(z) = \frac{p}{\eta_s} - \mathrm{i}\omega. \tag{2.7}$$

Here, $f(z)$ and $g(z)$ are called the Goursat functions (Goursat 1898) and can be determined from the boundary conditions. The Goursat functions are not unique; there is an additive degree of freedom in their definition. If we redefine $f(z)$ and $g(z)$ as

$$f(z) \mapsto f(z) + Pz + c, \quad g'(z) \mapsto g'(z) + \overline{c}, \tag{2.8}$$

where the constants P and c are real and complex, respectively, then all the physical quantities are unchanged.

Here, we denote the classical conjugate and Schwarz conjugate of a function $f(z)$ as

$$\overline{f}(\overline{z}) := \overline{f(z)}, \quad \overline{f}(z) := \overline{f(\overline{z})}, \tag{2.9}$$

respectively. Following from the definition of the stream function (2.3), the velocity as a complex function takes the form

$$u + \mathrm{i}v = -2\mathrm{i}\frac{\partial\psi}{\partial\overline{z}} = -f(z) + z\,\overline{f}'\big(\overline{z}\big) + \overline{g}'\big(\overline{z}\big), \tag{2.10}$$

where $f'(z)$ denotes the derivative of the function $f(z)$ with respect to z.

3. Problem formulation

We consider pressure-driven flow in a two-dimensional sharp-cornered cross-slot geometry with channel width $2h$, with equal inflows in two horizontal 'arms' and outflows in two vertical 'arms', as shown schematically in figure 1. We impose the no-slip condition on the boundaries of the cross-slot that satisfies

$$-\overline{f}(\overline{z}) + \overline{z}\,f'(z) + g'(z) = 0, \tag{3.1}$$

which is derived from (2.10). Due to mass conservation, the inlet and outlet fluxes should balance: we set the flux in each arm to be $Q > 0$. We can define a flow strength measure $U = 3Q/4h^3 > 0$; the maximum of the actual inlet and outlet velocities is $U_{max} = 3Q/4h = Uh^2$. We have plane Poiseuille flow at infinity of each 'arm' (in the far field of the four ends).

We decompose our cross-slot domain into five convex polygonal sub-domains, as shown in figure 2(*a*). Domains 1–4 are unbounded, and domain 5 is bounded, and the arrows show the directions of integration, which will be discussed later.

The flow in each of domains 1, 2 and 5 is symmetric about the x-axis ($y = 0$), which implies, from the definition of the Schwarz conjugate in (2.9), the symmetry conditions

$$\overline{f}(z) = f(z), \quad \overline{g}'(z) = g'(z). \tag{3.2}$$

Similarly, the flow in each of domains 3, 4 and 5 is symmetric about the y-axis ($x = 0$), giving the symmetry conditions

$$\overline{f}(z) = -f(-z), \quad \overline{g}'(z) = -g'(-z). \tag{3.3}$$

https://doi.org/10.1017/jfm.2025.10999 Published online by Cambridge University Press

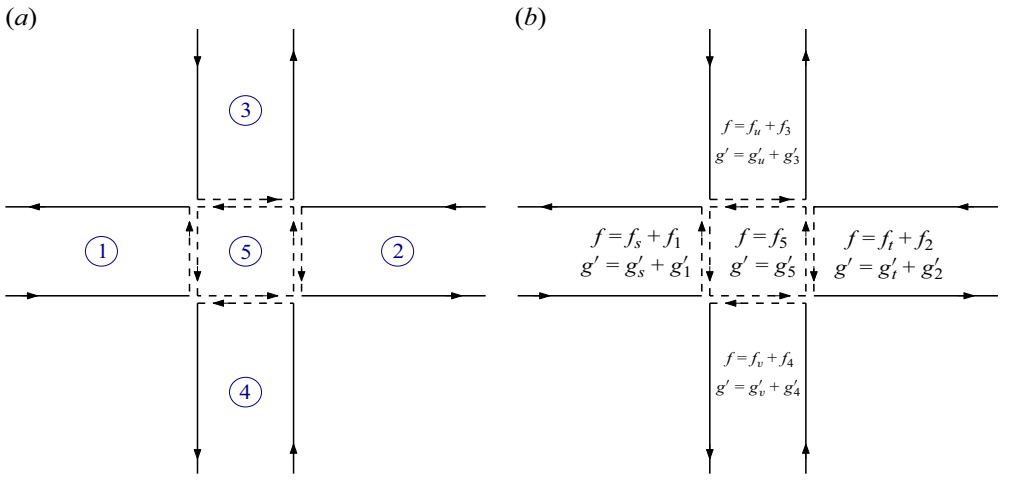


Figure 2. (*a*) Splitting of the whole cross-slot domain into five sub-domains (solid lines indicate real boundaries, dashed lines indicate transition between domain 5 and each of four 'arms'). (*b*) Expansions of the Goursat functions $f(z)$ and $g'(z)$ in each of five sub-domains.

4. Expansions of the Goursat functions

We expand the Goursat functions of each sub-domain into forcing terms, which capture the far-field behaviour of pressure-driven flow, and correction terms, which will be found through the UTM (Fokas 1997, 2008), as shown in figure 2(*b*). The details of the decomposition will be discussed later in this section.

4.1. *Domain 1*

The expansions of the Goursat functions of domain 1 take the form

$$f(z) = f_s(z) + f_1(z), \quad g'(z) = g'_s(z) + g'_1(z), \tag{4.1}$$

where $f_s(z)$ and $g'_s(z)$ are forcing terms, and $f_1(z)$ and $g'_1(z)$ are correction terms.

We write the forcing terms $f_s(z)$ and $g'_s(z)$ of domain 1 as

$$f_s(z) = -\frac{Uz^2}{4} + Pz + c_{in}, \quad g'_s(z) = \frac{Uz^2}{4} + Uh^2 + c_{in}. \tag{4.2}$$

Here, we add a linear contribution Pz with $P \in \mathbb{R}$ to domains 1 and 2, and additive parameters $c_{in} \in \mathbb{C}$ and $-c_{in}$ as constant terms to them, respectively. Without any loss of generality, we do not add any linear term to domains 3 and 4; however, it is still necessary to add complex additive parameters c_{out} and $-c_{out}$ to them, respectively, as shown below. From the symmetry condition (3.2) we can deduce that $c_{in} \in \mathbb{R}$, and it can also be deduced from (3.3) that $c_{out} \in \mathrm{i}\mathbb{R}$. We will see later that P has a connection with the value of the Couette correction, and that there is a relation between the constant parameters c_{in} and c_{out}.

The correction terms $f_1(z)$ and $g'_1(z)$ can then be represented in terms of so-called spectral functions, and can be found through the UTM (Fokas 1997, 2008), as shown below. It is easy to see that the correction terms decay well in the far field so that the integrals make no contribution in the far field, and the Cauchy integral formula can be generalised into unbounded domains. The correction term $f_1(z)$ can be represented in

https://doi.org/10.1017/jfm.2025.10999 Published online by Cambridge University Press

terms of spectral functions (Fokas & Kapaev 2003) as

$$f_1(z) = \frac{1}{2\pi}\left[\int_0^{\infty} \rho_1(k)\mathrm{e}^{\mathrm{i}kz}\,\mathrm{d}k + \int_0^{-\infty} \rho_2(k)\mathrm{e}^{\mathrm{i}kz}\,\mathrm{d}k + \int_0^{-\mathrm{i}\infty} \rho_3(k)\mathrm{e}^{\mathrm{i}kz}\,\mathrm{d}k\right], \tag{4.3}$$

with spectral functions of the form

$$\rho_1(k) = \int_{-\infty-\mathrm{i}h}^{-h-\mathrm{i}h} f_1(z)\mathrm{e}^{-\mathrm{i}kz}\,\mathrm{d}z, \quad \rho_2(k) = \int_{-h+\mathrm{i}h}^{-\infty+\mathrm{i}h} f_1(z)\mathrm{e}^{-\mathrm{i}kz}\,\mathrm{d}z, \tag{4.4a,b}$$

$$\rho_3(k) = \int_{-h-\mathrm{i}h}^{-h+\mathrm{i}h} f_1(z)\mathrm{e}^{-\mathrm{i}kz}\,\mathrm{d}z. \tag{4.4c}$$

According to Cauchy's theorem, the spectral functions satisfy the global relation

$$\rho_1(k) + \rho_2(k) + \rho_3(k) = 0, \quad \mathrm{Im}\,[k] \geq 0. \tag{4.5}$$

Similar to (4.3)–(4.5), the correction term $g_1'(z)$ can be written in terms of the spectral functions $\hat{\rho}_j(k)$, $j = 1, 2, 3$, with a similar global relation.

4.2. *Domains 2, 3 and 4*

Similar to domain 1, the Goursat functions of domain 2 can be expanded into

$$f(z) = f_t(z) + f_2(z), \quad g'(z) = g_t'(z) + g_2'(z), \tag{4.6}$$

where the forcing terms $f_t(z)$, $g_t'(z)$ are given by

$$f_t(z) = \frac{Uz^2}{4} + Pz - c_{in}, \quad g_t'(z) = -\frac{Uz^2}{4} - Uh^2 - c_{in}, \tag{4.7}$$

and the correction term $f_2(z)$ can be represented by

$$f_2(z) = \frac{1}{2\pi}\left[\int_0^{\infty} \sigma_1(k)\mathrm{e}^{\mathrm{i}kz}\,\mathrm{d}k + \int_0^{-\infty} \sigma_2(k)\mathrm{e}^{\mathrm{i}kz}\,\mathrm{d}k + \int_0^{\mathrm{i}\infty} \sigma_3(k)\mathrm{e}^{\mathrm{i}kz}\,\mathrm{d}k\right], \tag{4.8}$$

with the spectral functions

$$\sigma_1(k) = \int_{h-\mathrm{i}h}^{\infty-\mathrm{i}h} f_2(z)\mathrm{e}^{-\mathrm{i}kz}\,\mathrm{d}z, \quad \sigma_2(k) = \int_{\infty+\mathrm{i}h}^{h+\mathrm{i}h} f_2(z)\mathrm{e}^{-\mathrm{i}kz}\,\mathrm{d}z, \tag{4.9a,b}$$

$$\sigma_3(k) = \int_{h+\mathrm{i}h}^{h-\mathrm{i}h} f_2(z)\mathrm{e}^{-\mathrm{i}kz}\,\mathrm{d}z. \tag{4.9c}$$

The spectral functions satisfy the global relation

$$\sigma_1(k) + \sigma_2(k) + \sigma_3(k) = 0, \quad \mathrm{Im}\,[k] \leq 0. \tag{4.10}$$

Expressions similar to (4.8)–(4.10) can be written for $g_2'(z)$ (in terms of $\hat{\sigma}_j(k)$, $j = 1, 2, 3$).

The expansions of the Goursat functions of domain 3 take the form

$$f(z) = f_u(z) + f_3(z), \quad g'(z) = g_u'(z) + g_3'(z), \tag{4.11}$$

with forcing terms

$$f_u(z) = \frac{\mathrm{i}Uz^2}{4} + c_{out}, \quad g_u'(z) = \frac{\mathrm{i}Uz^2}{4} - \mathrm{i}Uh^2 - c_{out}, \tag{4.12}$$

and the correction term $f_3(z)$ can be written as

$$f_3(z) = \frac{1}{2\pi}\left[\int_0^{-\mathrm{i}\infty} \tau_1(k)\mathrm{e}^{\mathrm{i}kz}\,\mathrm{d}k + \int_0^{\mathrm{i}\infty} \tau_2(k)\mathrm{e}^{\mathrm{i}kz}\,\mathrm{d}k + \int_0^{\infty} \tau_3(k)\mathrm{e}^{\mathrm{i}kz}\,\mathrm{d}k\right], \tag{4.13}$$

https://doi.org/10.1017/jfm.2025.10999 Published online by Cambridge University Press

using the spectral functions

$$\tau_1(k) = \int_{h+\mathrm{i}h}^{h+\mathrm{i}\infty} f_3(z)\mathrm{e}^{-\mathrm{i}kz}\,\mathrm{d}z, \quad \tau_2(k) = \int_{-h+\mathrm{i}\infty}^{-h+\mathrm{i}h} f_3(z)\mathrm{e}^{-\mathrm{i}kz}\,\mathrm{d}z, \tag{4.14a,b}$$

$$\tau_3(k) = \int_{-h+\mathrm{i}h}^{h+\mathrm{i}h} f_3(z)\mathrm{e}^{-\mathrm{i}kz}\,\mathrm{d}z, \tag{4.14c}$$

and the global relation becomes

$$\tau_1(k) + \tau_2(k) + \tau_3(k) = 0, \quad \mathrm{Re}\,[k] \le 0. \tag{4.15}$$

Similar to (4.13)–(4.15), $g_3'(z)$ can be written in terms of $\hat{\tau}_j(k)$, $j = 1, 2, 3$, with a similar global relation.

Similarly, for the Goursat functions of domain 4, we write

$$f(z) = f_v(z) + f_4(z), \quad g'(z) = g_v'(z) + g_4'(z), \tag{4.16}$$

with forcing terms

$$f_v(z) = -\frac{\mathrm{i}Uz^2}{4} - c_{out}, \quad g_v'(z) = -\frac{\mathrm{i}Uz^2}{4} + \mathrm{i}Uh^2 + c_{out}, \tag{4.17}$$

and the representation of the correction term as

$$f_4(z) = \frac{1}{2\pi}\left[\int_0^{-\mathrm{i}\infty} \chi_1(k)\mathrm{e}^{\mathrm{i}kz}\,\mathrm{d}k + \int_0^{\mathrm{i}\infty} \chi_2(k)\mathrm{e}^{\mathrm{i}kz}\,\mathrm{d}k + \int_0^{-\infty} \chi_3(k)\mathrm{e}^{\mathrm{i}kz}\,\mathrm{d}k\right], \tag{4.18}$$

using spectral functions

$$\chi_1(k) = \int_{h-\mathrm{i}\infty}^{h-\mathrm{i}h} f_4(z)\mathrm{e}^{-\mathrm{i}kz}\,\mathrm{d}z, \quad \chi_2(k) = \int_{-h-\mathrm{i}\infty}^{-h-\mathrm{i}h} f_4(z)\mathrm{e}^{-\mathrm{i}kz}\,\mathrm{d}z, \tag{4.19a,b}$$

$$\chi_3(k) = \int_{h-\mathrm{i}h}^{-h-\mathrm{i}h} f_4(z)\mathrm{e}^{-\mathrm{i}kz}\,\mathrm{d}z. \tag{4.19c}$$

The global relation becomes

$$\chi_1(k) + \chi_2(k) + \chi_3(k) = 0, \quad \mathrm{Re}\,[k] \ge 0. \tag{4.20}$$

We can write expressions similar to (4.18)–(4.20) for $g_4'(z)$ in terms of $\hat{\chi}_j(k)$, $j = 1, 2, 3$.

4.3. *Domain 5*

Since domain 5 is a bounded sub-domain, the Goursat functions in domain 5 have correction terms only. Hence we have

$$f(z) = f_5(z), \quad g'(z) = g_5'(z). \tag{4.21}$$

Similarly, the correction term $f_5(z)$ can also be written in terms of spectral functions:

$$f_5(z) = \frac{1}{2\pi}\left[\int_0^{\infty} \upsilon_1(k)\mathrm{e}^{\mathrm{i}kz}\,\mathrm{d}k + \int_0^{-\mathrm{i}\infty} \upsilon_2(k)\mathrm{e}^{\mathrm{i}kz}\,\mathrm{d}k + \int_0^{-\infty} \upsilon_3(k)\mathrm{e}^{\mathrm{i}kz}\,\mathrm{d}k + \int_0^{\mathrm{i}\infty} \upsilon_4(k)\mathrm{e}^{\mathrm{i}kz}\,\mathrm{d}k\right], \tag{4.22}$$

https://doi.org/10.1017/jfm.2025.10999 Published online by Cambridge University Press

where the spectral functions are

$$\upsilon_1(k) = \int_{-h-\mathrm{i}h}^{h-\mathrm{i}h} f_5(z)\mathrm{e}^{-\mathrm{i}kz}\,\mathrm{d}z, \quad \upsilon_2(k) = \int_{h-\mathrm{i}h}^{h+\mathrm{i}h} f_5(z)\mathrm{e}^{-\mathrm{i}kz}\,\mathrm{d}z, \tag{4.23a,b}$$

$$\upsilon_3(k) = \int_{h+\mathrm{i}h}^{-h+\mathrm{i}h} f_5(z)\mathrm{e}^{-\mathrm{i}kz}\,\mathrm{d}z, \quad \upsilon_4(k) = \int_{-h+\mathrm{i}h}^{-h-\mathrm{i}h} f_5(z)\mathrm{e}^{-\mathrm{i}kz}\,\mathrm{d}z, \tag{4.23c,d}$$

and the global relation is

$$\upsilon_1(k) + \upsilon_2(k) + \upsilon_3(k) + \upsilon_4(k) = 0, \quad k \in \mathbb{C}. \tag{4.24}$$

Similar to (4.22)–(4.24), the correction term $g_5'(z)$ can be written in terms of the spectral functions $\hat{v}_j(k)$, $j = 1, 2, 3, 4$, with a similar global relation.

5. Spectral analysis

In this section, we will use the no-slip boundary condition (3.1) on the channel walls to obtain relations between the spectral functions.

5.1. *Domain 1*

Using the symmetry condition in (3.2) and the expansions (4.1), on the lower boundary $\overline{z} = z + 2\mathrm{i}h$ we have

$$-f_1(z + 2\mathrm{i}h) + (z + 2\mathrm{i}h)\, f_1'(z) + g_1'(z) = 0. \tag{5.1}$$

Similarly, on the upper boundary $\overline{z} = z - 2\mathrm{i}h$ we have

$$-f_1(z - 2\mathrm{i}h) + (z - 2\mathrm{i}h)\, f_1'(z) + g_1'(z) = 0. \tag{5.2}$$

Multiplying (5.1) by $\mathrm{e}^{-\mathrm{i}kz}$ and integrating along the lower boundary (in the arrow direction shown in figure 2), it can be shown that

$$\mathrm{e}^{-2kh}\,\rho_2(k) - \frac{\partial\,[k\rho_1(k)]}{\partial k} - 2kh\,\rho_1(k) + \hat{\rho}_1(k) + (-h + \mathrm{i}h)\, f_1(-h - \mathrm{i}h)\,\mathrm{e}^{-\mathrm{i}k(-h-\mathrm{i}h)} = 0. \tag{5.3}$$

Similarly, multiplying (5.2) by $\mathrm{e}^{-\mathrm{i}kz}$ and integrating along the upper boundary (in the arrow direction shown in figure 2), we can show that

$$\mathrm{e}^{2kh}\,\rho_1(k) - \frac{\partial\,[k\rho_2(k)]}{\partial k} + 2kh\,\rho_2(k) + \hat{\rho}_2(k) - (-h - \mathrm{i}h)\, f_1(-h + \mathrm{i}h)\,\mathrm{e}^{-\mathrm{i}k(-h+\mathrm{i}h)} = 0. \tag{5.4}$$

Adding (5.3) and (5.4), and using the global relation (4.5), we have

$$2\,[\sinh(2kh) - 2kh]\,\rho_1(k) = W_1(k), \quad \mathrm{Im}\,[k] \geq 0, \tag{5.5}$$

where

$$\begin{aligned} W_1(k) = {} & \left[\mathrm{e}^{-2kh} + 2kh\right]\rho_3(k) - \frac{\partial\,[k\,\rho_3(k)]}{\partial k} + \hat{\rho}_3(k) \\ & - (-h + \mathrm{i}h)\, f_1(-h - \mathrm{i}h)\,\mathrm{e}^{-\mathrm{i}k(-h-\mathrm{i}h)} \\ & + (-h - \mathrm{i}h)\, f_1(-h + \mathrm{i}h)\,\mathrm{e}^{-\mathrm{i}k(-h+\mathrm{i}h)}. \end{aligned} \tag{5.6}$$

5.2. *Domains 2, 3 and 4*

Using similar spectral analysis and the global relations (4.10), (4.15) and (4.20), respectively, we can deduce that

$$2\,[\sinh(2kh) - 2kh]\,\sigma_1(k) = W_2(k), \quad \mathrm{Im}\,[k] \leq 0, \tag{5.7}$$

https://doi.org/10.1017/jfm.2025.10999 Published online by Cambridge University Press

where

$$W_2(k) = \left[\mathrm{e}^{-2kh} + 2kh\right]\sigma_3(k) - \frac{\partial\,[k\,\sigma_3(k)]}{\partial k} + \hat{\sigma}_3(k) + (h + \mathrm{i}h)\; f_2\,(h - \mathrm{i}h)\,\mathrm{e}^{-\mathrm{i}k(h-\mathrm{i}h)} - (h - \mathrm{i}h)\; f_2\,(h + \mathrm{i}h)\,\mathrm{e}^{-\mathrm{i}k(h+\mathrm{i}h)}, \tag{5.8}$$

and that

$$2\left[\,\sinh\,(2\mathrm{i}kh) - 2\mathrm{i}kh\right]\tau_1(k) = W_3(k), \quad \mathrm{Re}\,[k] \le 0, \tag{5.9}$$

where

$$W_3(k) = \left[\mathrm{e}^{-2\mathrm{i}kh} + 2\mathrm{i}kh\right]\tau_3(k) - \frac{\partial\,[k\,\tau_3(k)]}{\partial k} - \hat{\tau}_3(k) + (-h + \mathrm{i}h)\; f_3\,(h + \mathrm{i}h)\,\mathrm{e}^{-\mathrm{i}k(h+\mathrm{i}h)} - (h + \mathrm{i}h)\; f_3\,(-h + \mathrm{i}h)\,\mathrm{e}^{-\mathrm{i}k(-h+\mathrm{i}h)}, \tag{5.10}$$

and finally that

$$2\,[\sinh\,(2\mathrm{i}kh) - 2\mathrm{i}kh]\;\chi_1(k) = W_4(k), \quad \mathrm{Re}\,[k] \ge 0, \tag{5.11}$$

where

$$W_4(k) = \left[\mathrm{e}^{-2\mathrm{i}kh} + 2\mathrm{i}kh\right]\chi_3(k) - \frac{\partial\,[k\,\chi_3(k)]}{\partial k} - \hat{\chi}_3(k) - (-h - \mathrm{i}h)\; f_4\,(h - \mathrm{i}h)\,\mathrm{e}^{-\mathrm{i}k(h-\mathrm{i}h)} + (h - \mathrm{i}h)\; f_4\,(-h - \mathrm{i}h)\,\mathrm{e}^{-\mathrm{i}k(-h-\mathrm{i}h)}. \tag{5.12}$$

More mathematical details of the spectral analysis of these sub-domains are given in Appendix A.

6. Continuity conditions

Imposing the continuity of velocity, pressure and vorticity along the transition between neighbouring sub-domains, we can obtain continuity conditions for the Goursat functions.

For the transition between domains 1 and 5, along $z = -h + \mathrm{i}y$, $y \in [-h, h]$, we have

$$f_s(z) + f_1(z) = f_5(z), \quad g_s'(z) + g_1'(z) = g_5'(z). \tag{6.1}$$

Similarly, between domains 2 and 5, along $z = h + \mathrm{i}y$, $y \in [-h, h]$, we have

$$f_5(z) = f_t(z) + f_2(z), \quad g_5'(z) = g_t'(z) + g_2'(z); \tag{6.2}$$

between domains 3 and 5, along $z = x + \mathrm{i}h$, $x \in [-h, h]$, we have

$$f_u(z) + f_3(z) = f_5(z), \quad g_u'(z) + g_3'(z) = g_5'(z); \tag{6.3}$$

and finally between domains 4 and 5, along $z = x - \mathrm{i}h$, $x \in [-h, h]$, we have

$$f_5(z) = f_v(z) + f_4(z), \quad g_5'(z) = g_v'(z) + g_4'(z). \tag{6.4}$$

7. Solution scheme

In this section, we formulate the linear system to calculate the Goursat functions along the transition between domain 5 and each of the four 'arms'. We will discuss three different possibilities: without the use of any symmetry condition, with the use of a symmetry

https://doi.org/10.1017/jfm.2025.10999 Published online by Cambridge University Press

condition in domain 5 only, and finally with the use of a symmetry condition in domain 5 and symmetry between each pair of opposite 'arms'. We will compare the results under these different conditions to ensure computational accuracy of our results, and investigate whether our transform approach can capture the symmetry conditions 'automatically', and whether this method can be used to solve Stokes flow problems in further complicated geometries.

After spectral analysis, we have the following system:

$$2\left[\sinh\left(2kh\right)-2kh\right]\rho_1(k)=W_1(k),\qquad \mathrm{Im}\left[k\right]\geq 0, \tag{7.1a}$$

$$2\left[\sinh\left(2kh\right)-2kh\right]\sigma_1(k)=W_2(k),\qquad \mathrm{Im}\left[k\right]\leq 0, \tag{7.1b}$$

$$2\left[\sinh\left(2\mathrm{i}kh\right)-2\mathrm{i}kh\right]\tau_1(k)=W_3(k),\qquad \mathrm{Re}\left[k\right]\leq 0, \tag{7.1c}$$

$$2\left[\sinh\left(2\mathrm{i}kh\right)-2\mathrm{i}kh\right]\chi_1(k)=W_4(k),\qquad \mathrm{Re}\left[k\right]\geq 0. \tag{7.1d}$$

Here, since the spectral functions $\rho_1(k)$, $\sigma_1(k)$, $\tau_1(k)$ and $\chi_1(k)$ are analytic in their corresponding spectral k-plane (half-plane), respectively, we have

$$W_1(k)=0 \quad \text{for } k\in\Sigma_1\equiv\{k:\mathrm{Im}\left[k\right]\geq 0\,|\,\sinh\left(2kh\right)-2kh=0\}, \tag{7.2a}$$

$$W_2(k)=0 \quad \text{for } k\in\Sigma_2\equiv\{k:\mathrm{Im}\left[k\right]\leq 0\,|\,\sinh\left(2kh\right)-2kh=0\}, \tag{7.2b}$$

$$W_3(k)=0 \quad \text{for } k\in\Sigma_3\equiv\{k:\mathrm{Re}\left[k\right]\leq 0\,|\,\sinh\left(2\mathrm{i}kh\right)-2\mathrm{i}kh=0\}, \tag{7.2c}$$

$$W_4(k)=0 \quad \text{for } k\in\Sigma_4\equiv\{k:\mathrm{Re}\left[k\right]\geq 0\,|\,\sinh\left(2\mathrm{i}kh\right)-2\mathrm{i}kh=0\}. \tag{7.2d}$$

We also have

$$\sinh\left(2kh\right)-2kh=O\left(k^3\right)\quad \text{as } k\to 0, \tag{7.3}$$

which indicates that

$$W_1\left(0\right)=W_1'\left(0\right)=W_1''\left(0\right)=0, \tag{7.4a}$$

$$W_2\left(0\right)=W_2'\left(0\right)=W_2''\left(0\right)=0, \tag{7.4b}$$

$$W_3\left(0\right)=W_3'\left(0\right)=W_3''\left(0\right)=0, \tag{7.4c}$$

$$W_4\left(0\right)=W_4'\left(0\right)=W_4''\left(0\right)=0. \tag{7.4d}$$

We have now reduced our problem to that of determining the values of $f(z)$ and $g'(z)$ along the transition between neighbouring sub-domains, i.e. along the four edges of domain 5. We now expand each of these in terms of Chebyshev polynomials:

$$f_5\left(z_1\left(s\right)\right)=\sum_{m=0}^{\infty}a_m\,T_m\left(s\right),\qquad g_5'\left(z_1\left(s\right)\right)=\sum_{m=0}^{\infty}A_m\,T_m\left(s\right), \tag{7.5a}$$

$$f_5\left(z_2\left(s\right)\right)=\sum_{m=0}^{\infty}b_m\,T_m\left(s\right),\qquad g_5'\left(z_2\left(s\right)\right)=\sum_{m=0}^{\infty}B_m\,T_m\left(s\right), \tag{7.5b}$$

$$f_5\left(z_3\left(s\right)\right)=\sum_{m=0}^{\infty}c_m\,T_m\left(s\right),\qquad g_5'\left(z_3\left(s\right)\right)=\sum_{m=0}^{\infty}C_m\,T_m\left(s\right), \tag{7.5c}$$

$$f_5\left(z_4\left(s\right)\right)=\sum_{m=0}^{\infty}d_m\,T_m\left(s\right),\qquad g_5'\left(z_4\left(s\right)\right)=\sum_{m=0}^{\infty}D_m\,T_m\left(s\right), \tag{7.5d}$$

where the four edges of domain 5 are parametrised in the obvious way in terms of a new variable s:

$$z_1\left(s\right)=hs-\mathrm{i}h,\qquad s\in\left[-1,\,1\right], \tag{7.6a}$$

$$z_2\left(s\right)=h+\mathrm{i}hs,\qquad s\in\left[-1,\,1\right], \tag{7.6b}$$

https://doi.org/10.1017/jfm.2025.10999 Published online by Cambridge University Press

$$z_3(s) = -hs + \mathrm{i}h, \quad s \in [-1, 1], \tag{7.6c}$$
$$z_4(s) = -h - \mathrm{i}hs, \quad s \in [-1, 1]. \tag{7.6d}$$

Here, $T_m(s) = \cos(m \cos^{-1}(s))$ is the mth Chebyshev polynomial of the first kind (Boyd 2000), and $\{a_m, b_m, c_m, d_m, A_m, B_m, C_m, D_m\}$ are the unknown coefficients that need to be calculated. According to (4.23), the spectral functions of domain 5 can then be expressed as

$$\upsilon_1(k) = \sum_{m=0}^{\infty} a_m [T_1(k, m)], \quad \hat{\upsilon}_1(k) = \sum_{m=0}^{\infty} A_m [T_1(k, m)], \tag{7.7a}$$
$$\upsilon_2(k) = \sum_{m=0}^{\infty} b_m [T_2(k, m)], \quad \hat{\upsilon}_2(k) = \sum_{m=0}^{\infty} B_m [T_2(k, m)], \tag{7.7b}$$
$$\upsilon_3(k) = \sum_{m=0}^{\infty} c_m [T_3(k, m)], \quad \hat{\upsilon}_3(k) = \sum_{m=0}^{\infty} C_m [T_3(k, m)], \tag{7.7c}$$
$$\upsilon_4(k) = \sum_{m=0}^{\infty} d_m [T_4(k, m)], \quad \hat{\upsilon}_4(k) = \sum_{m=0}^{\infty} D_m [T_4(k, m)], \tag{7.7d}$$

where

$$T_j(k, m) = \int_{-1}^{1} T_m(s)\, \mathrm{e}^{-\mathrm{i}kz_j(s)}\, z_j'(s)\, \mathrm{d}s, \quad j = 1, 2, 3, 4. \tag{7.8}$$

Using the continuity conditions (6.1)–(6.4), we can deduce that

$$\chi_3(k) = -\upsilon_1(k) + I_1(k), \quad \hat{\chi}_3(k) = -\hat{\upsilon}_1(k) + \hat{I}_1(k), \tag{7.9a}$$
$$\sigma_3(k) = -\upsilon_2(k) + I_2(k), \quad \hat{\sigma}_3(k) = -\hat{\upsilon}_2(k) + \hat{I}_2(k), \tag{7.9b}$$
$$\tau_3(k) = -\upsilon_3(k) + I_3(k), \quad \hat{\tau}_3(k) = -\hat{\upsilon}_3(k) + \hat{I}_3(k), \tag{7.9c}$$
$$\rho_3(k) = -\upsilon_4(k) + I_4(k), \quad \hat{\rho}_3(k) = -\hat{\upsilon}_4(k) + \hat{I}_4(k), \tag{7.9d}$$

where

$$I_1(k) = \int_{-h-\mathrm{i}h}^{h-\mathrm{i}h} f_v(z)\mathrm{e}^{-\mathrm{i}kz}\, \mathrm{d}z, \quad \hat{I}_1(k) = \int_{-h-\mathrm{i}h}^{h-\mathrm{i}h} g_v'(z)\mathrm{e}^{-\mathrm{i}kz}\, \mathrm{d}z, \tag{7.10a}$$
$$I_2(k) = \int_{h-\mathrm{i}h}^{h+\mathrm{i}h} f_t(z)\mathrm{e}^{-\mathrm{i}kz}\, \mathrm{d}z, \quad \hat{I}_2(k) = \int_{h-\mathrm{i}h}^{h+\mathrm{i}h} g_t'(z)\mathrm{e}^{-\mathrm{i}kz}\, \mathrm{d}z, \tag{7.10b}$$
$$I_3(k) = \int_{h+\mathrm{i}h}^{-h+\mathrm{i}h} f_u(z)\mathrm{e}^{-\mathrm{i}kz}\, \mathrm{d}z, \quad \hat{I}_3(k) = \int_{h+\mathrm{i}h}^{-h+\mathrm{i}h} g_u'(z)\mathrm{e}^{-\mathrm{i}kz}\, \mathrm{d}z, \tag{7.10c}$$
$$I_4(k) = \int_{-h+\mathrm{i}h}^{-h-\mathrm{i}h} f_s(z)\mathrm{e}^{-\mathrm{i}kz}\, \mathrm{d}z, \quad \hat{I}_4(k) = \int_{-h+\mathrm{i}h}^{-h-\mathrm{i}h} g_s'(z)\mathrm{e}^{-\mathrm{i}kz}\, \mathrm{d}z. \tag{7.10d}$$

7.1. *Without the use of any symmetry condition*

Using the continuity conditions (6.1)–(6.4), a linear system can be formulated with conditions in (4.24), (7.2) and (7.4), which allows us to calculate the unknown coefficients $\{a_m, b_m, c_m, d_m, A_m, B_m, C_m, D_m\}$ and the additive parameters P, c_{in} and c_{out}. In order to calculate these unknown coefficients and additive parameters, the infinite series expansions in (7.5) and (7.7) are truncated at suitable M. For moderate values of M,

https://doi.org/10.1017/jfm.2025.10999 Published online by Cambridge University Press

we find that the coefficients $\{a_m, b_m, c_m, d_m, A_m, B_m, C_m, D_m\}$ that we solve for decay reliably. However, if we truncate at too high a value of M, then we encounter difficulties with convergence: all physical quantities (stress and velocity components) show unphysical artefacts on the transition between neighbouring sub-domains. For this reason, we choose the truncation parameter to be $M = 8$, for which the ratios a_8/a_1, A_8/A_1, and so on are all of order at most 10^{-2}. Our choice here, using a Chebyshev basis to expand the Goursat functions along the four sides of domain 5, as shown in (7.5), yields convergent solutions with good accuracy in the domain interior. The system size, for $M = 8$ and 20 non-zero roots in each spectral k-plane, is 254×75. Solving this linear system takes a computational time of less than a second on a standard laptop.

The presence of sharp corners suggests that instead of Chebyshev expansions, one could employ tailor-made basis functions that account for the precise singularity at each corner. Such an approach was applied by Crowdy & Luca (2014), who used the UTM to analyse a biharmonic mixed boundary value problem; they introduced a uniformisation variable incorporating the known singular behaviour near corner points, and used it in a polynomial expansion to represent the unknown data. It was shown that spectrally accurate results were obtained. More recently, Colbrook and co-workers (Colbrook, Flyer & Fornberg 2018, 2019*a*,*b*; Colbrook 2020) proposed methods for addressing elliptic problems (for Laplace's, modified Helmholtz and Helmholtz equations) via the UTM in domains with corner singularities, which embed the known corner behaviour directly into the approximation scheme. While these strategies are relevant in the present context for the biharmonic equation, their implementation lies beyond the scope of this study. The use of a Chebyshev basis nevertheless provides good accuracy both in the domain interior and in the vicinity of the corners.

7.2. *With the use of a symmetry condition in domain 5 only*

If we use a symmetry condition in domain 5, then the global relation of domain 5 takes the form

$$\upsilon_1(k) + \upsilon_2(k) + \upsilon_1(-k) + \upsilon_2(-k) = 0, \quad k \in \mathbb{C}, \tag{7.11a}$$

$$\hat{\upsilon}_1(k) + \hat{\upsilon}_2(k) + \hat{\upsilon}_1(-k) + \hat{\upsilon}_2(-k) = 0, \quad k \in \mathbb{C}, \tag{7.11b}$$

$$\upsilon_3(k) + \upsilon_4(k) + \upsilon_3(-k) + \upsilon_4(-k) = 0, \quad k \in \mathbb{C}, \tag{7.11c}$$

$$\hat{\upsilon}_3(k) + \hat{\upsilon}_4(k) + \hat{\upsilon}_3(-k) + \hat{\upsilon}_4(-k) = 0, \quad k \in \mathbb{C}. \tag{7.11d}$$

The system of equations in (7.2), (7.4) and (7.11) allows us to calculate the unknown coefficients $\{a_m, b_m, c_m, d_m, A_m, B_m, C_m, D_m \mid m = 0, \ldots, M\}$ and the additive parameters P, c_{in} and c_{out}.

7.3. *With the use of a symmetry condition in domain 5 and symmetry between each pair of opposite 'arms'*

If we use the symmetry between domains 1 and 2, and the symmetry between domains 3 and 4, then the system of equations in (7.2) and (7.4), and the last two equations in (7.11), allow us to calculate the unknown coefficients $\{c_m, d_m, C_m, D_m \mid m = 0, \ldots, M\}$ and the additive parameters P, c_{in} and c_{out}.

More mathematical details of the analysis using these symmetry conditions are given in Appendix B.

The coefficients $\{a_m, b_m, c_m, d_m, A_m, B_m, C_m, D_m \mid m = 0, \ldots, M\}$ (with some or no symmetry conditions) or $\{c_m, d_m, C_m, D_m \mid m = 0, \ldots, M\}$ (with all symmetry conditions) and the additive parameters P, c_{in} and c_{out} have been computed; the results can be obtained within only a second on a standard laptop for $M = 8$, and it has been

https://doi.org/10.1017/jfm.2025.10999 Published online by Cambridge University Press

confirmed that the result is stable in terms of both the number of roots in the spectral k-planes and the truncation of Chebyshev expansions (choice of M). Within the limits of numerical precision, we obtained $c_{out} = \mathrm{i}c_{in}$, which corresponds to the symmetry between the inlets and outlets. After calculating the coefficients and the additive parameters, all the spectral functions (and therefore all the Goursat functions) can be calculated; we discuss these in the next section.

Under the above three conditions (with all, some or no symmetry conditions), we obtain the same solution within the limits of numerical precision, which indicates that our method is valid even without the symmetry conditions between different 'arms' so that it can be used to solve Stokes flow problems in further complicated geometries with sharp corners.

8. Further calculation of the Goursat functions and their derivatives

In this section, our aim is to calculate the Goursat functions $f(z)$ and $g'(z)$ and their derivatives in the interior of each of the sub-domains.

Using the expansions of the Goursat functions $f_5(z)$ and $g_5'(z)$ in the interior of domain 5 (e.g. (4.22) for $f_5(z)$) and the series expansions of the corresponding spectral functions in (7.7), the Goursat functions in the interior of domain 5 can be easily expressed in the form of integrals with coefficients that have already been obtained when solving the linear system. We can also obtain the first and second derivatives of the Goursat functions by differentiating (4.22) once or twice, and similarly expressing them in the form of integrals.

More careful analysis is necessary when computing the Goursat functions in the interior of each of the four 'arms' (e.g. domain 1). Similar to domain 5, we use the expansion of the Goursat function in (4.1) with the value of the additive parameters P and c_{in} that we have obtained when solving the linear system, and the expansion of the correction term $f_1(z)$ in (4.3). The spectral functions can be expressed from (4.5) and (7.1). Then we split the original integral into two terms: e.g. for the first term of the Goursat function $f_1(z)$ in domain 1, we have

$$\frac{1}{2\pi}\int_0^\infty \rho_1(k)\mathrm{e}^{\mathrm{i}kz}\,\mathrm{d}k = \frac{1}{2\pi}\int_0^\epsilon \rho_1(k)\mathrm{e}^{\mathrm{i}kz}\,\mathrm{d}k + \frac{1}{2\pi}\int_\epsilon^\infty \rho_1(k)\mathrm{e}^{\mathrm{i}kz}\,\mathrm{d}k, \tag{8.1}$$

where the second integral on the right-hand side can be easily expressed using the continuity conditions in (6.1) and (7.9) with the series expansions in (7.5) and (7.7). Then we can use (7.4) and local analysis near $k = 0$ to calculate the first integral on the right-hand side.

In order to calculate the correction terms of the Goursat function $g'(z)$ in the interior of each of the four 'arms' (e.g. $g_1'(z)$ in domain 1), we again use the expansion in the form of spectral functions, where the spectral function $\hat{\rho}_3(k)$ can be expressed directly using the continuity condition in (7.9) with the series expansion in (7.7). The other two spectral functions can be expressed from (5.3) and (5.4), respectively. Then the first two integrals can be split into several terms, and we can find that several of them have already been calculated when calculating the correction term $f_1(z)$ and its derivatives, and that the others can be calculated directly using the continuity conditions in (6.1) and (7.9) with the series expansions in (7.5) and (7.7), and the technique of integration by parts.

9. Computational results for physical quantities

We can compute all physical quantities of interest after we compute the Goursat functions and their derivatives. In this section, we will show the computational results for all physical quantities of interest, including pressure and Couette correction, velocity field

https://doi.org/10.1017/jfm.2025.10999 Published online by Cambridge University Press

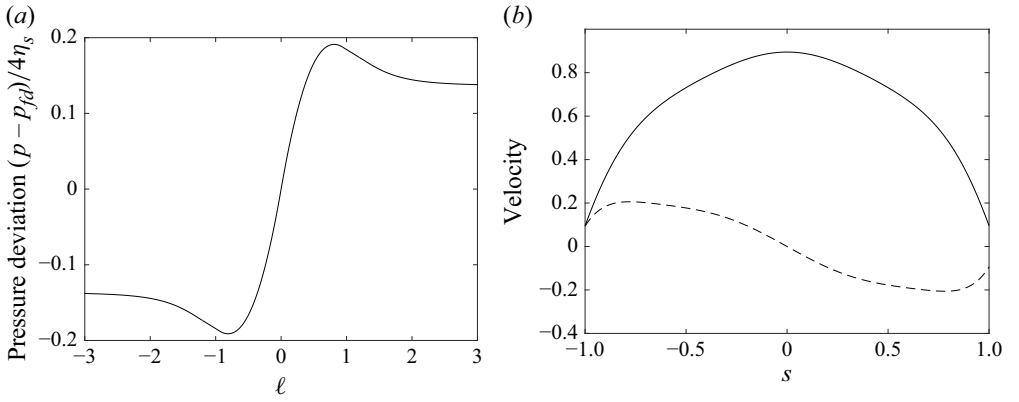


Figure 3. (*a*) The deviation of pressure from the linear variation corresponding to fully-developed unidirectional Poiseuille flow along the central line (from domain 1 to 5 to 3). (*b*) Velocity (solid line indicates real part u; dashed line indicates imaginary part v) along the transition between domains 1 and 5. All quantities are dimensionless.

and streamlines, and acceleration-like quantities such as stress, vorticity and flow-type parameter.

9.1. *Pressure and Couette correction*

We can deduce from (2.7) that the pressure takes the form

$$p = \mathrm{Re}\big[4\eta_s\, f'(z)\big]. \tag{9.1}$$

Then we plot the pressure deviation $(p - p_{fd})/4\eta_s$, where p_{fd} is the linear pressure associated with fully-developed Poiseuille flow in an inlet or outlet channel, along the central line (as shown in figure 1) of the sharp-cornered cross-slot geometry. This pressure deviation profile is shown in figure 3(*a*). The difference between the far-field inlets and outlets is the additive parameter P that we have solved from the linear system, which is part of the contribution to the Couette correction discussed below.

The Couette correction can be used to compare the pressure drop from the inlets to the outlets of the cross-slot geometry with fully developed flow in the straight channel. Defining the pressure drop from the inlets to the outlets of the cross-slot (e.g. from $z = -(L + h)$ to $z = \mathrm{i}(L + h)$, where L is large enough) as Δp, and the pressure drop from the inlet to the outlet of fully developed channel (from $z = -L$ to $z = L$) as Δp_{fd}, we can deduce that

$$\Delta p - \Delta p_{fd} = p(z = -(L + h)) - p(z = \mathrm{i}(L + h)) - 4\eta_s U L = 4\eta_s (Uh + P). \tag{9.2}$$

Since the wall stress takes the form

$$\sigma_w = \eta_s \left|\frac{\partial u}{\partial y}\right| (y = h) = 2\eta_s U h, \tag{9.3}$$

and the average velocity across the channel is $2Uh^2/3$, from $P \approx -0.3Uh$, which we have computed when solving the linear system, we can obtain the Couette correction C as

$$C = \frac{\Delta p - \Delta p_{fd}}{2\sigma_w} \approx 0.7, \tag{9.4}$$

which corresponds well with the numerical results of the Newtonian case shown in the graph of figure 14 in Rocha *et al.* (2009).

https://doi.org/10.1017/jfm.2025.10999 Published online by Cambridge University Press

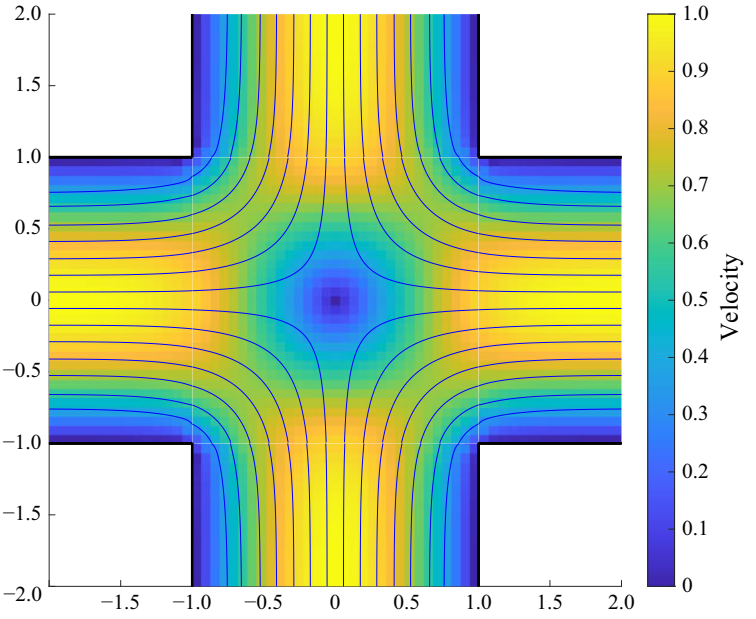


Figure 4. Dimensionless velocity field and streamlines of pressure-driven flow through the cross-slot.

9.2. *Velocity field and streamlines*

In figure 3(*b*), we show the velocity along the transition between domains 1 and 5, as computed from (2.10). As expected, the u velocity (crossing the transition line) is symmetric across the channel, and the v velocity (parallel to the transition line) is antisymmetric. The deviation from zero velocity at the corner is of order 10^{-1}. We can also compute the velocity field in the whole cross-slot. The resulting streamlines are shown in figure 4, which correspond well with the numerical results of the Newtonian case shown in the qualitative figure (figure 4) of Rocha *et al.* (2009).

9.3. *Acceleration-like quantities*

We define the strain rate tensor (also called the deformation rate tensor) as

$$\boldsymbol{E} := \frac{1}{2}\left(\boldsymbol{\nabla U} + (\boldsymbol{\nabla U})^{\mathrm{T}}\right), \tag{9.5}$$

and the vorticity tensor as

$$\boldsymbol{\Omega} := \frac{1}{2}\left(\boldsymbol{\nabla U} - (\boldsymbol{\nabla U})^{\mathrm{T}}\right). \tag{9.6}$$

The flow-type parameter $\xi \in [-1, 1]$ is defined (Lee *et al.* 2007; Davoodi *et al.* 2019) as

$$\xi := \frac{\|\boldsymbol{E}\| - \|\boldsymbol{\Omega}\|}{\|\boldsymbol{E}\| + \|\boldsymbol{\Omega}\|}, \tag{9.7}$$

where

$$\|\boldsymbol{E}\| := \sqrt{\frac{\boldsymbol{E} : \boldsymbol{E}}{2}}, \quad \|\boldsymbol{\Omega}\| := \sqrt{\frac{\boldsymbol{\Omega} : \boldsymbol{\Omega}}{2}}. \tag{9.8}$$

Here, $\xi = -1$ corresponds to a solid-like rotational flow, $\xi = 0$ to a simple shear flow, and $\xi = 1$ to a pure extensional flow, and for intermediate values of ξ, we have a mixture of

https://doi.org/10.1017/jfm.2025.10999 Published online by Cambridge University Press

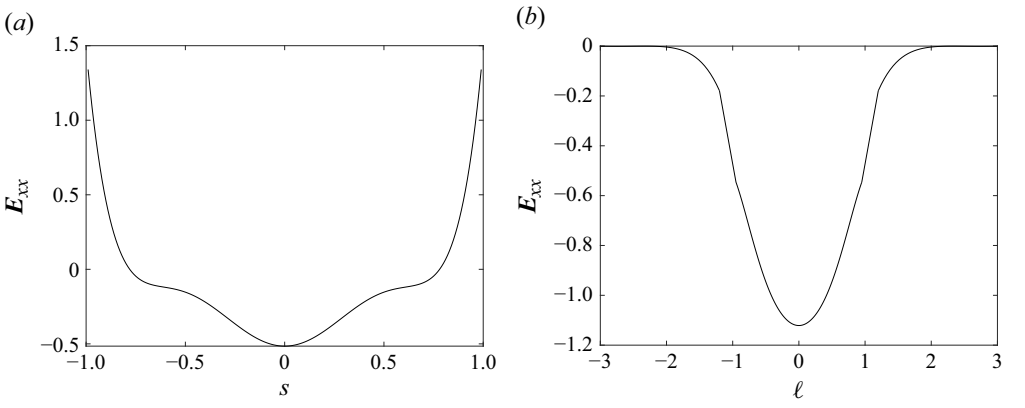


Figure 5. Dimensionless strain rate $\boldsymbol{E}_{xx} = -\boldsymbol{E}_{yy}$ (*a*) along the transition between domains 1 and 5, and (*b*) along the central line (from domain 1 to 5 to 3).

different flow types. Defining $F(z, \overline{z}) := \overline{z}\, f''(z) + g''(z)$, we have

$$\boldsymbol{E}_{xx} = -\boldsymbol{E}_{yy} = \frac{1}{2}\big(\boldsymbol{E}_{xx} - \boldsymbol{E}_{yy}\big) = \mathrm{Re}\,[F\,(z, \overline{z})], \tag{9.9a}$$

$$\boldsymbol{E}_{xy} = \boldsymbol{E}_{yx} = -\mathrm{Im}\,[F\,(z, \overline{z})], \tag{9.9b}$$

$$\boldsymbol{\Omega}_{xy} = -\boldsymbol{\Omega}_{yx} = \mathrm{i}\big[f'(z) - \overline{f}'\big(\overline{z}\big)\big], \tag{9.9c}$$

$$\xi = 1 - \frac{2\big|f'(z) - \overline{f}'\big(\overline{z}\big)\big|}{\big|F\big(z, \overline{z}\big)\big| + \big|f'(z) - \overline{f}'\big(\overline{z}\big)\big|}. \tag{9.9d}$$

Figures 5(*a*) and 5(*b*) show the behaviour of the strain rate $\boldsymbol{E}_{xx} = -\boldsymbol{E}_{yy}$ along the transition between domains 1 and 5, and along the central line, respectively; these both agree with the numerical results of the sharp-cornered Newtonian case shown in figures 5, 6 and 10 of Rocha *et al.* (2009).

Figures 6(*a*) and 7 display the strain rate $\boldsymbol{E}_{xy}$ along the transition between domains 1 and 5 and in the whole cross-slot, respectively.

The vorticity $\boldsymbol{\Omega}_{xy}$ along the transition between domains 1 and 5, and in the whole cross-slot, and the flow-type parameter ξ along the transition between domains 1 and 5, all correspond well with the numerical results of the Newtonian case shown in the qualitative figures in figure 7 of Davoodi *et al.* (2019); these quantities are shown in figures 6 and 8.

On the central line, we have also computed the strain rate $\boldsymbol{E}_{xy}$ (always 0 within the limits of numerical precision), vorticity $\boldsymbol{\Omega}_{xy}$ (always 0 within the limits of numerical precision) and flow-type parameter ξ (always 1 within the limits of numerical precision). Here, both $\boldsymbol{\Omega}_{xy}$ and ξ also correspond well with figure 7 of Davoodi *et al.* (2019).

10. Discussion and future directions

We have analysed Stokes flow through a symmetric sharp-cornered cross-slot geometry using the UTM. We split the non-convex domain into five convex sub-domains, and analysed the boundary conditions in each of the sub-domains to obtain relations between the so-called spectral functions. The analysis of the relations between the spectral functions, and the use of global relations, offered information on a reduced set of unknown spectral functions at special points in the spectral k-plane. Using series expansions to represent unknown boundary data, we formulated and solved a low-order linear system

https://doi.org/10.1017/jfm.2025.10999 Published online by Cambridge University Press

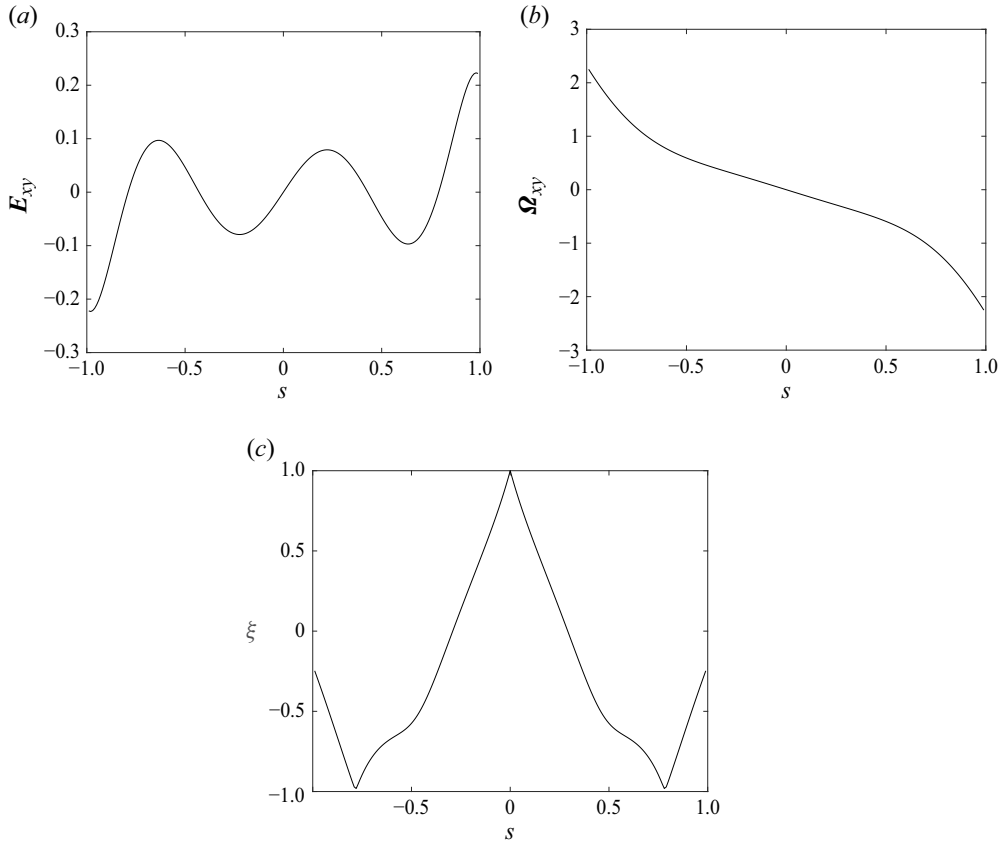


Figure 6. (*a*) Strain rate $\boldsymbol{E}_{xy}$, (*b*) vorticity $\boldsymbol{\Omega}_{xy}$ and (*c*) flow-type parameter ξ along the transition between domains 1 and 5. All quantities are dimensionless.

for the unknown coefficients. All the spectral functions followed from back-substitution into the spectral relations. With all, some or no symmetry conditions, we obtained the same solution within the limits of numerical precision, which ensured that our results were accurate, and our transform approach can capture the symmetry conditions 'automatically'.

One of the main advantages of our transform approach over full numerical simulations is that all physical quantities of interest can be computed from the solution of low-order linear systems, with great computational speed as well as computational accuracy in solving the Stokes flow problem in a complicated geometry. Another advantage is that one can calculate the quantities of interest everywhere in unbounded geometries without meshing for some preset regions or truncating at some finite distance. All the aforementioned features are a result of the quasi-analytical nature of our solution. It should also be noted that we have considered symmetric flow and exploited the symmetry to obtain conditions between the Goursat functions, but it is straightforward to adapt our analysis to analyse antisymmetric or even general flow with different inlets and outlets, as well as different channel widths.

We have used the UTM to compute all the physical quantities of interest in order to investigate the use of this method in solving a complicated geometry. Without the requirements of any extra local asymptotic analysis near the sharp corners, our transform approach with the Chebyshev expansions representing the unknown boundary data is

https://doi.org/10.1017/jfm.2025.10999 Published online by Cambridge University Press

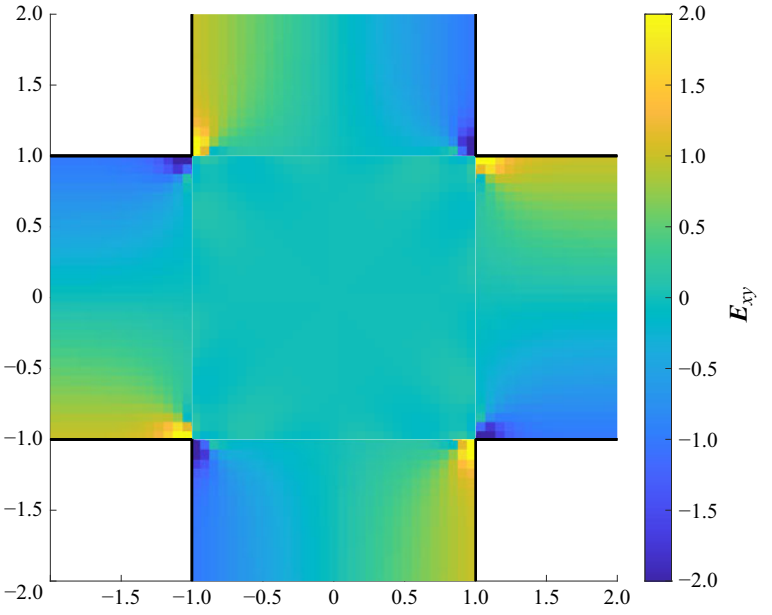


Figure 7. Dimensionless strain rate $\boldsymbol{E}_{xy}$ of pressure-driven flow through the cross-slot.

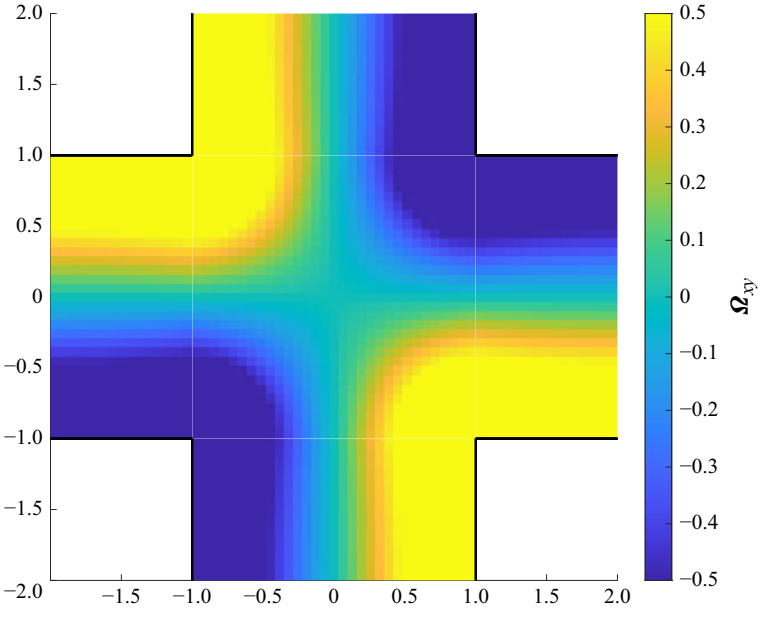


Figure 8. Dimensionless vorticity $\boldsymbol{\Omega}_{xy}$ of pressure-driven flow through the cross-slot.

able to capture the asymptotic behaviour of the velocity at and near the sharp corners 'automatically'.

As expected, there is considerable symmetry in the computed velocity fields, with a stagnation point at the centre of the geometry, and the velocity is maximal at the centreline of the inlets and outlets. The rate of strain shows a more complicated behaviour, with

https://doi.org/10.1017/jfm.2025.10999 Published online by Cambridge University Press

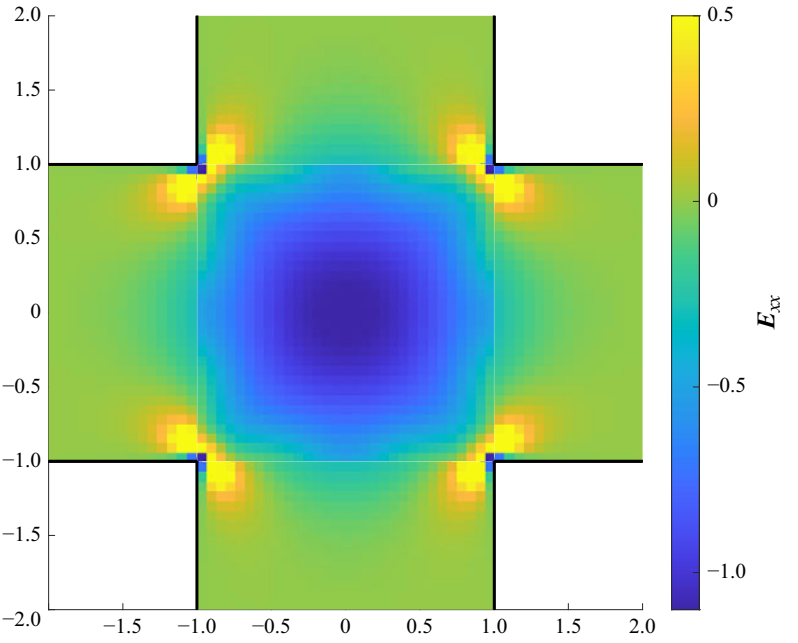


Figure 9. Dimensionless strain rate $\boldsymbol{E}_{xx} = -\boldsymbol{E}_{yy}$ of pressure-driven flow through the cross-slot.

rapid oscillations in shear stress near each corner singularity, which agree with near-field asymptotics; and we are able to compute the Couette correction (extra pressure drop due to the junction) as 0.7.

As expected, the accuracy of our numerical results is at its weakest close to the four sharp corners, where the flow is singular. Indeed, it is known (Moffatt 1964; Hawa & Rusak 2002; Pozrikidis 2011) that if we look close to one of the corners and use r to represent distance from the corner, velocities scale like $r^{\lambda-1}$, and therefore strain rates and stresses diverge as $r^{\lambda-2}$, where $\lambda \approx 1.54448374$. We have no difficulty with velocity here, but our results for acceleration-like quantities (stress, vorticity, flow-type parameter, etc.) are less accurate very close to the corners, hence a more careful analysis is required; this remains a topic for future investigation. This behaviour is illustrated in figure 9 (for strain rate $\boldsymbol{E}_{xx} = -\boldsymbol{E}_{yy}$) and figure 10 (for flow-type parameter ξ, which is derived from strain rate as defined in (9.7)). Our approach has difficulty in capturing the correct asymptotic behaviour very close to the corners for these quantities, but this concerns only the nearest grid points from the corners. All the physical quantities away from the corners, in which we are more interested, are well-behaved, and the computational results are accurate. Our results are in agreement with the full simulation results of the Newtonian case shown in Rocha *et al.* (2009) and Davoodi *et al.* (2019). To conclude, we obtain the whole velocity profile, including the asymptotic behaviour near the corners, with very smooth streamlines, and all the other quantities far from the corner very accurately. We expect that our method can be adapted to further complicated geometries with sharp corners in the future. For example, we could introduce different widths of inlets and outlets as extra parameters to capture an asymmetric cross-slot.

Funding. This research received no specific grant from any funding agency, commercial or not-for-profit sectors.

Declaration of interests. The authors report no conflict of interest.

https://doi.org/10.1017/jfm.2025.10999 Published online by Cambridge University Press

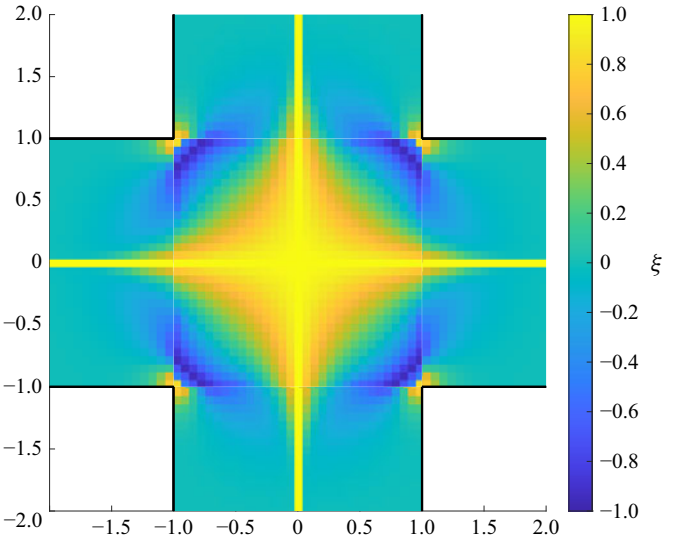


Figure 10. Flow-type parameter ξ of pressure-driven flow through the cross-slot.

Author contributions. X.J. carried out all the calculations and wrote the computational code with all technical details. H.J.W. and E.L. contributed equally to some technical details of the methods. All three authors contributed to the writing of the paper: X.J. original draft, H.J.W. and E.L. refinement.

Appendix A. Mathematical details of spectral analysis of domains 2, 3 and 4

A.1. *Domain 2*

Using the symmetry condition in (3.2) and the expansions (4.6), on the lower boundary $\overline{z} = z + 2\mathrm{i}h$ we have

$$-f_2\,(z+2\mathrm{i}h) + (z+2\mathrm{i}h)\;f_2'(z) + g_2'(z) = 0. \tag{A1}$$

Similarly, on the upper boundary $\overline{z} = z - 2\mathrm{i}h$ we have

$$-f_2\,(z-2\mathrm{i}h) + (z-2\mathrm{i}h)\;f_2'(z) + g_2'(z) = 0. \tag{A2}$$

Multiplying (A1) by $\mathrm{e}^{-\mathrm{i}kz}$ and integrating along the lower boundary (in the arrow direction shown in figure 2), it can be shown that

$$\mathrm{e}^{-2kh}\,\sigma_2(k) - \frac{\partial\,[k\sigma_1(k)]}{\partial k} - 2kh\sigma_1(k) + \hat{\sigma}_1(k) - (h+\mathrm{i}h)\;f_2\,(h-\mathrm{i}h)\,\mathrm{e}^{-\mathrm{i}k(h-\mathrm{i}h)} = 0. \tag{A3}$$

Similarly, multiplying (A2) by $\mathrm{e}^{-\mathrm{i}kz}$ and integrating along the upper boundary (in the arrow direction shown in figure 2), we have

$$\mathrm{e}^{2kh}\,\sigma_1(k) - \frac{\partial\,[k\sigma_2(k)]}{\partial k} + 2kh\sigma_2(k) + \hat{\sigma}_2(k) + (h-\mathrm{i}h)\;f_2\,(h+\mathrm{i}h)\,\mathrm{e}^{-\mathrm{i}k(h+\mathrm{i}h)} = 0. \tag{A4}$$

Adding (A3) and (A4), and using the global relation (4.10), we obtain (5.7).

https://doi.org/10.1017/jfm.2025.10999 Published online by Cambridge University Press

A.2. *Domain 3*

Using the symmetry condition in (3.3) and the expansions (4.11), on the right-hand boundary $\overline{z} = -z + 2h$ we have

$$f_3\,(z-2h) - (z-2h)\,f_3'(z) + g_3'(z) = 0. \tag{A5}$$

Similarly, on the left-hand boundary $\overline{z} = -z - 2h$ we have

$$f_3\,(z+2h) - (z+2h)\,f_3'(z) + g_3'(z) = 0. \tag{A6}$$

Multiplying (A5) by $\mathrm{e}^{-\mathrm{i}kz}$ and integrating along the right-hand boundary (in the arrow direction shown in figure 2), we can obtain that

$$-\mathrm{e}^{-2\mathrm{i}kh}\,\tau_2(k) + \frac{\partial\,[k\,\tau_1(k)]}{\partial k} + 2\mathrm{i}kh\,\tau_1(k) + \hat{\tau}_1(k) + (-h+\mathrm{i}h)\,f_3\,(h+\mathrm{i}h)\,\mathrm{e}^{-\mathrm{i}k(h+\mathrm{i}h)} = 0. \tag{A7}$$

Similarly, multiplying (A6) by $\mathrm{e}^{-\mathrm{i}kz}$ and integrating along the left-hand boundary (in the arrow direction shown in figure 2), we have

$$-\mathrm{e}^{2\mathrm{i}kh}\,\tau_1(k) + \frac{\partial\,[k\,\tau_2(k)]}{\partial k} - 2\mathrm{i}kh\,\tau_2(k) + \hat{\tau}_2(k) - (h+\mathrm{i}h)\,f_3\,(-h+\mathrm{i}h)\,\mathrm{e}^{-\mathrm{i}k(-h+\mathrm{i}h)} = 0. \tag{A8}$$

Adding (A7) and (A8) and using the global relation (4.15) gives (5.9).

A.3. *Domain 4*

Using the symmetry condition in (3.3) and the expansions (4.16), on the right-hand boundary $\overline{z} = -z + 2h$ we have

$$f_4\,(z-2h) - (z-2h)\,f_4'(z) + g_4'(z) = 0. \tag{A9}$$

Similarly, on the left-hand boundary $\overline{z} = -z - 2h$ we have

$$f_4\,(z+2h) - (z+2h)\,f_4'(z) + g_4'(z) = 0. \tag{A10}$$

Multiplying (A9) by $\mathrm{e}^{-\mathrm{i}kz}$ and integrating along the right-hand boundary (in the arrow direction shown in figure 2), we can show that

$$-\mathrm{e}^{-2\mathrm{i}kh}\,\chi_2(k) + \frac{\partial\,[k\,\chi_1(k)]}{\partial k} + 2\mathrm{i}kh\,\chi_1(k) + \hat{\chi}_1(k) - (-h-\mathrm{i}h)\,f_4\,(h-\mathrm{i}h)\,\mathrm{e}^{-\mathrm{i}k(h-\mathrm{i}h)} = 0. \tag{A11}$$

Similarly, multiplying (A10) by $\mathrm{e}^{-\mathrm{i}kz}$ and integrating along the left-hand boundary (in the arrow direction shown in figure 2), we have

$$-\mathrm{e}^{2\mathrm{i}kh}\,\chi_1(k) + \frac{\partial\,[k\,\chi_2(k)]}{\partial k} - 2\mathrm{i}kh\,\chi_2(k) + \hat{\chi}_2(k) + (h-\mathrm{i}h)\,f_4\,(-h-\mathrm{i}h)\,\mathrm{e}^{-\mathrm{i}k(-h-\mathrm{i}h)} = 0. \tag{A12}$$

Adding (A11) and (A12), and using the global relation (4.20), we obtain (5.11).

Appendix B. Mathematical details of analysis on the symmetry condition in domain 5 and symmetry between each pair of opposite 'arms'

If we use the symmetry condition in domain 5 as

$$f_5(z) = -f_5(-z), \quad g_5'(z) = -g_5'(-z), \tag{B1}$$

then we know that

$$\upsilon_1(k) = \upsilon_3\,(-k)\,, \quad \upsilon_2(k) = \upsilon_4\,(-k)\,, \quad \hat{\upsilon}_1(k) = \hat{\upsilon}_3\,(-k)\,, \quad \hat{\upsilon}_2(k) = \hat{\upsilon}_4\,(-k)\,, \tag{B2}$$

https://doi.org/10.1017/jfm.2025.10999 Published online by Cambridge University Press

which indicates that

$$f_5(z) = \frac{1}{2\pi}\left[\int_0^{\infty} \upsilon_3\,(-k)\,\mathrm{e}^{\mathrm{i}kz}\,\mathrm{d}k + \int_0^{-\mathrm{i}\infty} \upsilon_4\,(-k)\,\mathrm{e}^{\mathrm{i}kz}\,\mathrm{d}k + \int_0^{-\infty} \upsilon_3(k)\mathrm{e}^{\mathrm{i}kz}\,\mathrm{d}k + \int_0^{\mathrm{i}\infty} \upsilon_4(k)\mathrm{e}^{\mathrm{i}kz}\,\mathrm{d}k\right], \tag{B3}$$

$$g_5'(z) = \frac{1}{2\pi}\left[\int_0^{\infty} \hat{\upsilon}_3\,(-k)\,\mathrm{e}^{\mathrm{i}kz}\,\mathrm{d}k + \int_0^{-\mathrm{i}\infty} \hat{\upsilon}_4\,(-k)\,\mathrm{e}^{\mathrm{i}kz}\,\mathrm{d}k + \int_0^{-\infty} \hat{\upsilon}_3(k)\mathrm{e}^{\mathrm{i}kz}\,\mathrm{d}k + \int_0^{\mathrm{i}\infty} \hat{\upsilon}_4(k)\mathrm{e}^{\mathrm{i}kz}\,\mathrm{d}k\right], \tag{B4}$$

and gives the global relation (7.11).

If we use the symmetry between domains 1 and 2, then we can show that

$$f_2\,(z_2) = -f_1\,(z_1)\,, \quad g_2'\,(z_2) = -g_1'\,(z_1), \tag{B5}$$

where z_1 is in domain 1, z_2 is in domain 2, and $z_1 = -z_2$. Similarly, if we use the symmetry between domains 3 and 4, then we have

$$f_4\,(z_4) = -f_3\,(z_3)\,, \quad g_4'\,(z_4) = -g_3'\,(z_3), \tag{B6}$$

where z_3 is in domain 3, z_4 is in domain 4, and $z_3 = -z_4$.

References

Abrahams, I.D., Davis, A.M.J. & Llewellyn Smith, S.G. 2008 Asymmetric channel divider in Stokes flow. *SIAM J. Appl. Math.* **68** (5), 1439–1463.

Alves, M.A. 2008 Design of a cross-slot flow channel for extensional viscosity measurements. In *AIP Conference Proceedings*, pp. 240–242. American Institute of Physics.

Arratia, P.E., Thomas, C.C., Diorio, J. & Gollub, J.P. 2006 Elastic instabilities of polymer solutions in cross-channel flow. *Phys. Rev. Lett.* **96** (14), 144502.

Boyd, J.P. 2000 *Chebyshev and Fourier Spectral Methods*, 2nd edn. Courier Corporation.

Brubeck, P.D. & Trefethen, L.N. 2022 Lightning Stokes solver. *SIAM J. Sci. Comput.* **44** (3), A1205–A1226.

Colbrook, M.J. 2020 Extending the unified transform: curvilinear polygons and variable coefficient PDEs. *IMA J. Numer. Anal.* **40** (2), 976–1004.

Colbrook, M.J., Ayton, L.J. & Fokas, A.S. 2019*a* The unified transform for mixed boundary condition problems in unbounded domains. *Proc. R. Soc. A* **475** (2222), 20180605.

Colbrook, M.J., Flyer, N. & Fornberg, B. 2018 On the Fokas method for the solution of elliptic problems in both convex and non-convex polygonal domains. *J. Comput. Phys.* **374**, 996–1016.

Colbrook, M.J., Fokas, T.S. & Hashemzadeh, P. 2019*b* A hybrid analytical–numerical technique for elliptic PDEs. *SIAM J. Sci. Comput.* **41** (2), A1066–A1090.

Costa, S. & Trefethen, L.N. 2023 AAA-least squares rational approximation and solution of Laplace problems. In *European Congress of Mathematics*, pp. 511–534. European Mathematical Society Press.

Crowdy, D.G. 2013*a* Exact solutions for cylindrical 'slip–stick' Janus swimmers in Stokes flow. *J. Fluid Mech.* **719**, R2.

Crowdy, D.G. 2013*b* Surfactant-induced stagnant zones in the Jeong–Moffatt free surface Stokes flow problem. *Phys. Fluids* **25** (9), 092104.

Crowdy, D.G. & Brzezicki, S.J. 2017 Analytical solutions for two-dimensional Stokes flow singularities in a no-slip wedge of arbitrary angle. *Proc. R. Soc. A* **473** (2202), 20170134.

Crowdy, D.G. & Davis, A.M.J. 2013 Stokes flow singularities in a two-dimensional channel: a novel transform approach with application to microswimming. *Proc. R. Soc. A* **469** (2157), 20130198.

Crowdy, D.G. & Fokas, A.S. 2004 Explicit integral solutions for the plane elastostatic semi-strip. *Proc. R. Soc. A* **460** (2045), 1285–1309.

Crowdy, D.G. & Luca, E. 2014 Solving Wiener–Hopf problems without kernel factorization. *Proc. R. Soc. A* **470** (2170), 20140304.

Crowdy, D.G. & Samson, O. 2010 Stokes flows past gaps in a wall. *Proc. R. Soc. A* **466** (2121), 2727–2746.

Cruz, F.A., Poole, R.J., Afonso, A.M., Pinho, F.T., Oliveira, P.J. & Alves, M.A. 2014 A new viscoelastic benchmark flow: stationary bifurcation in a cross-slot. *J. Non-Newtonian Fluid Mech.* **214**, 57–68.

https://doi.org/10.1017/jfm.2025.10999 Published online by Cambridge University Press

DAVIS, A.M.J. 1993 Periodic blocking in parallel shear or channel flow at low Reynolds number. *Phys. Fluids* **5** (4), 800–809.

DAVOODI, M., DOMINGUES, A.F. & POOLE, R.J. 2019 Control of a purely elastic symmetry-breaking flow instability in cross-slot geometries. *J. Fluid Mech.* **881**, 1123–1157.

DEAN, W.R. & MONTAGNON, P.E. 1949 On the steady motion of viscous liquid in a corner. *Math. Proc. Camb. Phil. Soc.* **45** (3), 389–394.

DIMAKOS, M. & FOKAS, A.S. 2015 The Poisson and the biharmonic equations in the interior of a convex polygon. *Stud. Appl. Math.* **134** (4), 456–498.

DYLLA-SPEARS, R., TOWNSEND, J.E., JEN-JACOBSON, L., SOHN, L.L. & MULLER, S.J. 2010 Single-molecule sequence detection via microfluidic planar extensional flow at a stagnation point. *Lab Chip* **10** (12), 1543–1549.

FOKAS, A.S. 1997 A unified transform method for solving linear and certain nonlinear PDEs. *Proc. R. Soc. A* **453** (1962), 1411–1443,

FOKAS, A.S. 2008 *A Unified Approach to Boundary Value Problems, CBMS-NSF Regional Conference Series in Applied Mathematics*, vol. 78. Society for Industrial and Applied Mathematics.

FOKAS, A.S. & KAPAEV, A.A. 2003 On a transform method for the Laplace equation in a polygon. *IMA J. Appl. Math.* **68** (4), 355–408.

GALINDO-ROSALES, F.J., ALVES, M.A. & OLIVEIRA, M.S.N. 2013 Microdevices for extensional rheometry of low viscosity elastic liquids: a review. *Microfluid. Nanofluid.* **14**, 1–19.

GOPAL, A. & TREFETHEN, L.N. 2019 Solving Laplace problems with corner singularities via rational functions. *SIAM J. Numer. Anal.* **57** (5), 2074–2094.

GOURSAT, E. 1898 Sur l'équation $\Delta\Delta u = 0$. *Bull. Soc. Math. Fr.* **26**, 236–237.

HAWA, T. & RUSAK, Z. 2002 Numerical–asymptotic expansion matching for computing a viscous flow around a sharp expansion corner. *Theor. Comput. Fluid Dyn.* **15** (5), 265–281.

HAWARD, S.J., OLIVEIRA, M.S.N., ALVES, M.A. & MCKINLEY, G.H. 2012 Optimized cross-slot flow geometry for microfluidic extensional rheometry. *Phys. Rev. Lett.* **109** (12), 128301.

HELLOU, M. & BACH, T.D.P. 2011 Stokes flow in a junction of two-dimensional orthogonal channels. *Z. Angew. Math. Phys.* **62**, 135–147.

HOWISON, S. 2005 *Practical Applied Mathematics: Modelling, Analysis, Approximation*. Cambridge University Press.

JEONG, J.-T. 2001*a* Slip boundary condition on an idealized porous wall. *Phys. Fluids* **13** (7), 1884–1890.

JEONG, J.-T. 2001*b* Slow viscous flow in a partitioned channel. *Phys. Fluids* **13** (6), 1577–1582.

JOSEPH, D.D. 1977 The convergence of biorthogonal series for biharmonic and Stokes flow edge problems. Part I. *SIAM J. Appl. Math.* **33** (2), 337–347.

JOSEPH, D.D. & STURGES, L. 1978 The convergence of biorthogonal series for biharmonic and Stokes flow edge problems. Part II. *SIAM J. Appl. Math.* **34** (1), 7–26.

KIM, M.-U. & CHUNG, M.K. 1984 Two-dimensional slow viscous flow past a plate midway between an infinite channel. *J. Phys. Soc. Japan* **53** (1), 156–166.

KRÜGER, T., KUSUMAATMAJA, H., KUZMIN, A., SHARDT, O., SILVA, G. & VIGGEN, E.M. 2017 *The Lattice Boltzmann Method, Graduate Texts in Physics*, vol. 10. Springer.

LANGLOIS, W.E. 1964 *Slow Viscous Flow*. Springer.

LEE, J.S., DYLLA-SPEARS, R., TECLEMARIAM, N.P. & MULLER, S.J. 2007 Microfluidic four-roll mill for all flow types. *Appl. Phys. Lett.* **90** (7), 074103.

LOGG, A., MARDAL, K.-A. & WELLS, G. 2012 *Automated Solution of Differential Equations by the Finite Element Method: The FEniCS Book*. Lecture Notes in Computational Science and Engineering, vol. 84, Springer Science & Business Media.

LUCA, E. & CROWDY, D.G. 2018 A transform method for the biharmonic equation in multiply connected circular domains. *IMA J. Appl. Math.* **83** (6), 942–976.

LUCA, E. & LLEWELLYN SMITH, S.G. 2018 Stokes flow through a two-dimensional channel with a linear expansion. *Q. J. Mech. Appl. Math.* **71** (4), 441–462.

MANZ, A., LEE, A.P. & WHEELER, A.R. 2021 *Lab on a Chip* – past, present, and future. *Lab Chip* **21** (7), 1197–1198.

MELESHKO, V.V. 2003 Selected topics in the history of the two-dimensional biharmonic problem. *Appl. Mech. Rev.* **56** (1), 33–85.

MOFFATT, H.K. 1964 Viscous and resistive eddies near a sharp corner. *J. Fluid Mech.* **18** (1), 1–18.

NAKATSUKASA, Y., SÈTE, O. & TREFETHEN, L.N. 2018 The AAA algorithm for rational approximation. *SIAM J. Sci. Comput.* **40** (3), A1494–A1522.

OCKENDON, H. & OCKENDON, J.R. 1995 *Viscous Flow*. Cambridge University Press.

https://doi.org/10.1017/jfm.2025.10999 Published online by Cambridge University Press

ODELL, J.A. & CARRINGTON, S.P. 2006 Extensional flow oscillatory rheometry. *J. Non-Newtonian Fluid Mech.* **137** (1–3), 110–120.
PHILLIPS, T.N. 1989 Singular matched eigenfunction expansions for Stokes flow around a corner. *IMA J. Appl. Math.* **42** (1), 13–26.
POOLE, R.J., ALVES, M.A. & OLIVEIRA, P.J. 2007 Purely elastic flow asymmetries. *Phys. Rev. Lett.* **99** (16), 164503.
POZRIKIDIS, C. 1987 Creeping flow in two-dimensional channels. *J. Fluid Mech.* **180**, 495–514.
POZRIKIDIS, C. 1992 *Boundary Integral and Singularity Methods for Linearized Viscous Flow*. Cambridge University Press.
POZRIKIDIS, C. 2011 *Introduction to Theoretical and Computational Fluid Dynamics*. Oxford University Press.
ROCHA, G.N., POOLE, R.J., ALVES, M.A. & OLIVEIRA, P.J. 2009 On extensibility effects in the cross-slot flow bifurcation. *J. Non-Newtonian Fluid Mech.* **156** (1–2), 58–69.
ROURE, G., ZINCHENKO, A.Z. & DAVIS, R.H. 2024 Dynamics and active mixing of a droplet in a Stokes trap. *J. Fluid Mech.* **985**, A15.
SETCHI, A., MESTEL, A.J., PARKER, K.H. & SIGGERS, J.H. 2013 Low-Reynolds-number flow through two-dimensional shunts. *J. Fluid Mech.* **723**, 21–39.
SQUIRES, T.M. & QUAKE, S.R. 2005 Microfluidics: fluid physics at the nanoliter scale. *Rev. Mod. Phys.* **77** (3), 977–1026.
STRIKWERDA, J.C. 1984 Finite difference methods for the Stokes and Navier–Stokes equations. *SIAM J. Sci. Stat. Comput.* **5** (1), 56–68.
TAVAKOL, B., FROEHLICHER, G., HOLMES, D.P. & STONE, H.A. 2017 Extended lubrication theory: improved estimates of flow in channels with variable geometry. *Proc. R. Soc. A* **473** (2206), 20170234.
WANG, Z. & KELLEY, S.O. 2025 Microfluidic technologies for enhancing the potency, predictability and affordability of adoptive cell therapies. *Nat. Biomed. Engng* **9**, 803–821.
XU, Y., WANG, Z., LI, C., TIAN, S. & DU, W. 2025 Droplet microfluidics: unveiling the hidden complexity of the human microbiome. *Lab Chip* **25**, 1128–1148.
XUE, Y., PAYNE, S.J. & WATERS, S.L. 2025 Stokes flows in a two-dimensional bifurcation. *R. Soc. Open Sci.* **12** (1), 241392.
XUE, Y., WATERS, S.L. & TREFETHEN, L.N. 2024 Computation of two-dimensional Stokes flows via lightning and AAA rational approximation. *SIAM J. Sci. Comput.* **46** (2), A1214–A1234.
YEO, L.Y., CHANG, H.-C., CHAN, P.P.Y. & FRIEND, J.R. 2011 Microfluidic devices for bioapplications. *Small* **7** (1), 12–48.

https://doi.org/10.1017/jfm.2025.10999 Published online by Cambridge University Press